Journal of
Instrumentation

Development of a neutron/gamma diagnostic for RFX-mod2

Published by IOP Publishing for Sissa Medialab

Received: *February 24, 2026*
Accepted: *April 15, 2026*
Published: *May 5, 2026*

International Conference on Fusion Reactor Diagnostics: the Burning Plasma Era
Varenna, Italy
1–5 September 2025

2026 JINST 21 C05003

Development of a neutron/gamma diagnostic for RFX-mod2

F. Guiotto[a,b,d,*] **A. Dal Molin**[d] **L. Cordaro**[b] **M. Zuin**[b] **D. Rigamonti**[d] **O. Putignano**[d] **G. Croci**[c,d,e] **G. Grosso**[d] **L. Stevanato**[f] **C. Fontana**[g] **J.K. Anderson**[h] **N. Fonnesu**[i] **P. Franz**[b] **E. Perelli Cippo**[d] **M. Tardocchi**[d,e] **and A. Muraro**[d]

[a] *Centro Ricerche Fusione (CRF) - University of Padova, C.so Stati Uniti 4, 35127, Padova, Italy*
[b] *Consorzio RFX (CNR, ENEA, INFN, University of Padova, Acciaierie Venete SpA), C.so Stati Uniti 4, 35127, Padova, Italy*
[c] *Department of Physics 'G. Occhialini', University of Milano-Bicocca, Piazza della Scienza 3, Milan, 20125, Italy*
[d] *Institute for Plasma Science and Technology, National Research Council, Via Roberto Cozzi 53, Milan, 20125, Italy*
[e] *INFN, Section of Milano-Bicocca, Piazza della Scienza 3, Milan, 20125, Italy*
[f] *Finapp S.p.A., Via del Commercio, 27, 35036, Padova (PD), Italy*
[g] *European Commission, Joint Research Centre (JRC), Rue du Champ de Mars 21, 1050 Brussels, Belgium*
[h] *Department of Physics, University of Wisconsin-Madison, 2320 Chamberlin Hall, 1150 University Avenue, Madison, WI 53706, U.S.A.*
[i] *ENEA, Nuclear Department, Via E. Fermi, 45, 00044, Frascati, Rome, Italy*

E-mail: federico.guiotto@phd.unipd.it

Abstract: Magnetic Confinement Fusion aims to provide a virtually limitless, low-carbon energy source by harnessing nuclear fusion reactions of light nuclei under extreme temperature and pressure conditions, where matter exists as plasma. Magnetic Reconnection (MR) events are fast transient phenomena which directly impact plasma stability, energy losses, and overall efficiency of fusion devices, making their study relevant for the realization of commercial fusion energy. The world's largest Reversed-Field Pinch (RFP) fusion device is currently under development in Padova, Italy, and is called RFX-mod2. In this work, the development of a neutron/gamma diagnostic system for RFX-mod2 is presented. The diagnostic system aims primarily at obtaining experimental information

*Corresponding author.

https://doi.org/10.1088/1748-0221/21/05/C05003

on ion and electron acceleration to suprathermal energies driven by MR events. However, it could also be useful for other purposes, such as enabling neutron yield estimation and, in future RFX-mod2 tokamak discharges, the study of runaway electrons.

The main results of neutron and gamma-ray measurements related to MR events, performed in the past at RFX-mod and the Madison Symmetric Torus (MST), are briefly summarized. Their main limitations are identified and the requirements for the new neutron/gamma diagnostic are outlined.

The three-dimensional CAD (Computer Aided Design) model of the diagnostic system is presented, along with the need to develop a detector prototype to obtain experimental data at RFX-mod2 before assembling and commissioning the complete diagnostic system. An experimental characterization of the detector prototype is presented, including a neutron/gamma discrimination test.

KEYWORDS: Neutron detectors (cold, thermal, fast neutrons); Nuclear instruments and methods for hot plasma diagnostics; Scintillators, scintillation and light emission processes (solid, gas and liquid scintillators); Spectrometers

2026 JINST 21 C05003

Contents

2026 JINST 21 C05003

1 Introduction

1.1 RFX-mod2 and magnetic reconnection events

In the context of Magnetic Confinement Fusion (MCF) plasmas, Magnetic Reconnection (MR) events [1] are impulsive phenomena that involve the breaking and reconnection of magnetic field lines, leading to a reconfiguration of the magnetic field topology corresponding to a state of lower magnetic energy. Magnetic energy is converted into kinetic and thermal energy of the plasma, and is typically observed as acceleration of particles to non-thermal velocities [2] and generation of waves and turbulence [3, 4]. MR events directly impact plasma stability, energy losses, and overall efficiency of fusion devices, making their study important for the development of commercial fusion energy [5, 6]. In Reversed-Field Pinch (RFP) devices [7], such as RFX-mod [8] and MST [9], prominent manifestations of MR were observed, sometimes involving large-scale magnetic reconnection and global reorganization of the magnetic field configuration (e.g., from Quasi-Single-Helicity states towards Multiple-Helicity States [4, 7, 10]). A phenomenological analysis of multiple RFX-mod2 RFP discharges [10] identified abrupt decreases of the reversal parameter F as a recurrent signature of MR events. In a RFP, the F parameter:

$$F = \frac{B_\phi(a)}{\langle B_\phi \rangle}, \tag{1.1}$$

quantifies the degree of toroidal field $\left(B_\phi\right)$ reversal at the plasma edge [7]. In equation (1.1), a is the plasma minor radius, and the average $\left\langle B_\phi \right\rangle$ is computed over the plasma cross-section.

In deuterium plasmas, neutrons are produced through the d(d,n)^{3}He reaction, with a cross-section that is highly sensitive to the energies of the deuterons involved. Past measurements at MST [11, 12] indicated that, during MR events, tens of KJ of magnetic energy are released in $\sim 100\,\mu s$, leading to the acceleration of ions to suprathermal energies and ultimately to a significant increase in the neutron emission, measured as an increase in neutron rates at the detectors.

Soft X-ray (SXR) measurements at MST also revealed electron acceleration driven by MR events, with an energization process that favored particle motion perpendicular to the magnetic field lines [13, 14]. This was in agreement with ion energization observations at MST, which also suggested anisotropy favoring a perpendicular heating mechanism [11]. These results suggested that the cause of energization could be a turbulent mechanism rather then the development of an electric field with subsequent runaway electrons generation [14].

RFX-mod experiments also shown MR events correlated with ion heating and bursts of neutron and gamma-ray rates lasting $\approx 1\,ms$ [15–17].

The upgrade of RFX-mod (RFX-mod2 [18]) is expected to have a first wall made of graphite tiles with a thickness of 18 mm, a major radius = 2.0 m and minor radius = 0.5 m. The first wall is expected to be surrounded by a stabilizing Copper shell (3 mm thick), which is enclosed in a vacuum tight support structure (VTSS). The VTSS is expected to include 150 view ports and to embed a set of 4×48 saddle coils for real-time control of MHD instabilities [18]. Moreover, like RFX-mod, the device is designed to operate not only as a RFP, but also in tokamak and ultra-low q configurations [19–21]. Strong emphasis is placed on the expansion of the diagnostic suite [22, 23], including the development of SXR and neutron/gamma diagnostics to study the acceleration of ions and electrons to suprathermal energies. The development of the SXR diagnostic based on Gas Electron Multiplier (SXR-GEM) detectors was already presented in ref. [24], while the development of the new neutron/gamma diagnostic is presented in this paper.

This paper is organized as follows: section 2 summarizes the main results of past neutron and gamma measurements performed at RFX-mod and MST and related to MR events. Their main limitations are identified and it is discussed how the proposed neutron/gamma diagnostic system could address these gaps. Section 3 identifies the neutron/gamma diagnostic requirements based on past experimental experience at RFX-mod and MST. Then, it presents the three-dimensional Computer Aided Design (CAD) model of the diagnostic system and the foreseen photodetectors. Finally, the need to develop a prototype detector is presented. An experimental characterization of the prototype detector for neutron measurements, including a neutron/gamma discrimination test, is presented in section 4. Conclusions are provided in section 5.

2 Past measurements and main gaps

2.1 Neutron/gamma measurements at RFX-mod

During past deuterium discharges at RFX-mod, neutron and gamma count rates were measured and discriminated using a diagnostic system made of 2 scintillators: an organic NE213 liquid scintillator (now commercially available as "EJ-301" [25]), and an inorganic NaI(Tl) scintillator [26]. Both scintillators were coupled to H8500 flat-panel photomultiplier tubes (FP-PMTs) [15–17]. Anodic

2026 JINST 21 C05003

signals coming from both detectors were fed into a CAEN DT5751 digitizer (10 bits, 1 GS/s). Digital pulse processing algorithms were implemented in an FPGA to collect timestamps, perform Pulse Shape Discrimination (PSD) [26] and to store a voltage waveform for each event. The FP-PMT bias voltage was set to 850 Volts [17].

Both detectors were placed as close as possible to the machine to maximize the neutron flux. Specifically, they were placed at the equatorial plane, in front of a CF-250 porthole made of Zinc Selenide (ZnSe) [16, 17].

Each detector was enclosed in a 4 cm thick polyethylene box, itself surrounded by a metal box to reduce electromagnetic disturbances at the detector position. High Voltage (HV) and coaxial signal cables were isolated and shielded using conductive braided shielding and dielectric sleeving to minimize electromagnetic interference. The digitizer and HV power supply were positioned 1 m from the detector, inside a separate metal box, and connected via optical fibers to a computer located in an adjacent room [17].

A detailed description of the experimental setup can be found in ref. [17].

The standard PSD method based on pulse integration over a short and long gate[1] was used to discriminate neutron pulses from gamma pulses.

In 2014, neutron and gamma count rates were measured in 1185 shots of RFX-mod over 7 months of experimental campaign in both tokamak and RFP configurations [17]. Neutron and gamma bursts were observed at RFX-mod and a correlation of these bursts with MR events was suggested [15–17]. In addition, gamma and neutron fluxes were measured as the plasma current (I_p) was varied from 0.4 MA to 1.5 MA, corresponding to a parametric scan of the input ohmic power. Despite significant data scatter, both neutron and gamma fluxes exhibited a marked increase at higher ohmic input power levels.[2]

To investigate the dependence of gamma emission on plasma conditions, gamma energy spectra were also measured at RFX-mod, in different plasma configurations and I_p regimes.[3] In the RFP configuration, the continuum part of the energy spectrum was associated with Bremsstrahlung photons, generated by electrons accelerated to high energies during MR events. Conversely, in the tokamak configuration, it was hypothesized that Bremsstrahlung photons could have been generated by runaway electrons [16].

2.2 Neutron/gamma measurements at MST

In 2018, measurements of neutrons and gamma rays were performed at MST, during RFP deuterium plasma operations [12]. The measurement system comprised 5 EJ-309 liquid scintillators for neutron detection and 1 solid NaI(Tl) scintillator for gamma detection. Each scintillator was coupled to a FP-PMT. Each detector was individually shielded against non-direct gamma radiation using lead disks ($\approx$ 4 cm lateral shielding) and against non-direct neutrons using polyethylene ($\approx$ 7.5 cm lateral shielding). The output anode signals were fed into a CAEN DT5725 (14-bit, 250 MS/s) digitizer, equipped with algorithms for real-time analysis (e.g., PSD with the standard method based on pulse integration in a short and a long gate) of each individual scintillation event [12]. The PMTs were operated at relatively low voltage ($\sim$1 kV), in order to mitigate saturation effects, by means of a CAEN DT5533E HV power supply module. Each scintillator was characterized for its neutron and gamma

[1] Such as the one that will be presented in section 4.

[2] The reader may refer to figure 8.15 of ref. [17].

[3] The reader may refer to figure 4 of ref. [16].

2026 JINST 21 C05003

response prior to the measurements at MST [12]. The latter were performed during several MST discharges and revealed bursts of neutron and gamma count rates temporally correlated with MR events. An example is shown in figure 1(a), corresponding to a MST discharge without neutral beam injection. The figure displays the time evolution of the plasma current I_p, the loop voltage V_{loop},[4] the reversal parameter F, and the central chord line averaged electron density n_e, followed by five rows showing the count rate of each EJ-309 scintillator, and the final row showing the NaI(Tl) scintillator count rate. The EJ-309 signals comes from neutron-induced events (shown in red and discriminated through PSD) and gamma-induced events, while the NaI(Tl) signal is expected to be dominated by gamma-induced events. The black signals in the figure indicate the total rate, i.e., all events induced in the scintillators, independently from the interacting particle type. The figure suggests a correlation between sharp peaks in the V_{loop} signal, sharp drops in the F signal (indicative of MR events), and bursts of neutrons and gamma rates measured with the scintillators.

To investigate correlation of signals among different plasma discharges and to estimate the characteristic time scales of neutron bursts associated with MR events, a conditional averaging procedure was applied to approximately 160 MR events.

MR events were identified from the $F(t)$ signals, where t indicates the time. Only events corresponding to the deepest drops ($\Delta F \sim 0.1$) were retained, as these are expected to be associated with stronger MR activity. Furthermore, only events with comparable baseline values of F and plasma current I_p were selected.

For each event, the reference time t_{rec} was defined as the time corresponding to the minimum of the F drop. For each signal, a 10 ms time window centered at t_{rec} was extracted and re-expressed in terms of the shifted time variable

$$t' = t - t_{\text{rec}}.$$

Denoting by N_{MR} the number of selected MR events, the conditional average of a generic signal X was computed as

$$\langle X(t') \rangle = \frac{1}{N_{\text{MR}}} \sum_{i=1}^{N_{\text{MR}}} X_i(t'_i), \tag{2.1}$$

where $t'_i = t - t_{\text{rec},i}$ is the shifted time variable for the i-th MR event.

The results, shown in figure 1(b), indicate a correlation among the I_p spike, the F drop, and the increase in neutron count rate. The neutron count rate enhancement persists for approximately 3 ms before returning close to the baseline level.

2.3 Main gaps in RFX-mod measurements

Most RFX-mod measurements of the past were affected by artificial silent phases, during which the detector count rate signals were absent for the majority of the discharge time. An example of such a silent phase can be found in figure 8.13 of ref. [17]. The reason for these silent phases was not fully understood at the time, but represented an important limitation of the measurements.

Moreover, both RFX-mod and MST past measurements focused on neutron counting rather than neutron spectroscopy. Therefore, for these devices, the energy spectra of d-d neutrons are not available

[4] V_{loop} is the transformer-driven voltage that is used to sustain the plasma current (I_p) in a MCF device.

2026 JINST 21 C05003

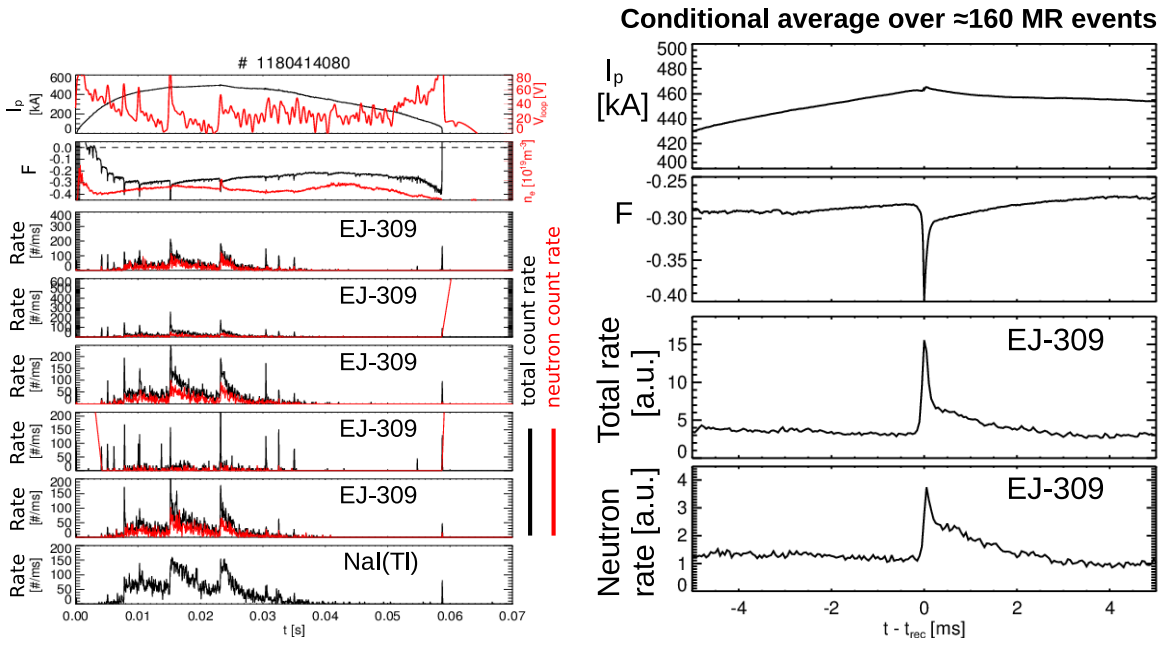

(a) (b)

Figure 1. Panel (a): Time evolution of plasma parameters and detector signals during an MST discharge without NBI (#1180414080). From top to bottom, the shown signals are: I_p, V_{loop}, F, n_e, the rates of the five EJ-309 scintillators, and the rate of the NaI(Tl) scintillator. The scintillator rates are expressed in counts per ms. Panel (b): Conditional average over ≈ 160 MR events. From top to bottom: I_p, F, total count rates, and neutron count rates (discriminated through the standard PSD method based on pulse integration in a short and a long gate). The horizontal axis is expressed in terms of the shifted time variable $t' = t - t_{\text{rec}}$ (in ms).

in the current literature. However, neutron spectroscopy is useful to select counts associated mostly to unscattered neutrons and to investigate the possible presence of high-energy tails in the neutron spectrum (indicative of suprathermal ion populations in the plasma).

Finally, past neutron measurements at RFX-mod were characterized by a single line of sight. Conversely, having more lines of sight could provide valuable spatial information on the increase in neutron flux. This could be useful for studying ion transport during MR events, potentially identifying a preferred direction of acceleration [11] at RFX-mod2, perhaps allowing a deeper understanding of the underlying mechanism.

3 Diagnostic design

3.1 Diagnostic requirements

The observations outlined above highlighted the need for a diagnostic system with high count-rate capability for RFX-mod2. In addition, the use of Silicon Photomultipliers (SiPMs) instead of PMTs or FP-PMTs was preferred to ensure a cautious approach toward reliable operation in the presence of strong magnetic fields at the detector locations (in the order of hundreds of mT).

Proper energy resolution for neutrons, and adequate shielding from non-direct neutrons and gamma-rays to obtain a basic level of spatial resolution, are desirable for RFX-mod2.

2026 JINST 21 C05003

Finally, the digitizer should be positioned at a sufficient distance from the device, ideally in an adjacent room, to mitigate possible issues associated with electromagnetic interference.

The neutron/gamma diagnostic proposed in this work is designed to address these needs. Moreover, it was proposed to use this diagnostic in combination with the same diagnostic system based on EJ-309 and NaI(Tl) detectors that were installed at MST in 2018 (section 2.2), providing higher plasma coverage, redundancy, and higher rates.

3.2 CAD model

For the RFX-mod2 neutron/gamma diagnostic, three view ports (internal, central, and external) located in the bottom part of the poloidal sector 12D are available. This is the same sector in which the SXR-GEM diagnostic [24] will be positioned. Specifically, the SXR-GEM will be located in the upper part of the sector 12D, viewing the plasma from the upper-central and upper-external view ports [24].

The three bottom view ports are located in correspondence to the three lines of sight (LOSs) of the neutron diagnostic. The latter are defined by the shielding that will be employed to reduce the contributions from non-direct neutrons and gamma rays to the count rate.

Each LOS is engineered to allow detector replacement from the bottom part of the support and shielding structures, ensuring flexibility in adapting the diagnostic to the specific operational scenario and experimental target. Two types of compact detectors can be interchangeably mounted in each LOS:

1. EJ-276D [27–31], square geometry, dimensions $1'' \times 1'' \times 4''$, intended for neutron and gamma counting at RFX-mod2. It is characterized by relatively high neutron-detection efficiency, but limited energy-resolution capability.

2. $LaCl_3$:Ce [32–35], which provides good spectroscopic performance but exhibits a lower neutron-detection efficiency. It is intended as a neutron and gamma spectrometer for RFX-mod2.

Past measurements at MST [11] reported neutron yields in the range of 10^8–10^{10} n/s. Although higher yields are expected at RFX-mod2 due to its capability to reach higher plasma currents, the radiation fluxes at the detector positions may still be insufficient to achieve adequate counting statistics on ms or sub-ms time scales. Therefore, to maximize the neutron flux, it was decided to place the detectors as close as possible (within the engineering constraints) to the RFX-mod2 vessel. A support structure that was used for the past RFX-mod polarimeter system will now be used as the support structure for the detectors and their associated shielding.

A detailed CAD model of the diagnostic system was produced in CATIA [36].

The CAD model showing the RFX-mod2 poloidal sector, the diagnostic with the full shielding structure, and the main geometrical parameters, is reported in figure 2.

3.3 Support structure, shielding, and installation concept

A bottom view of the CAD model assembly, showing the support structure for the detectors, their shielding, and the accessible region of the detectors, is shown in figure 3. The shielding structure is modular, composed of several layers of 5% borated polyethylene employed for non-direct neutron moderation and subsequent absorption of thermalized neutrons, and of several layers of lead disks embedded within the polyethylene structure, employed for the attenuation of non-direct gamma-rays. For the installation, this modularity becomes crucial, as few layers can act as placeholders to align

2026 JINST 21 C05003

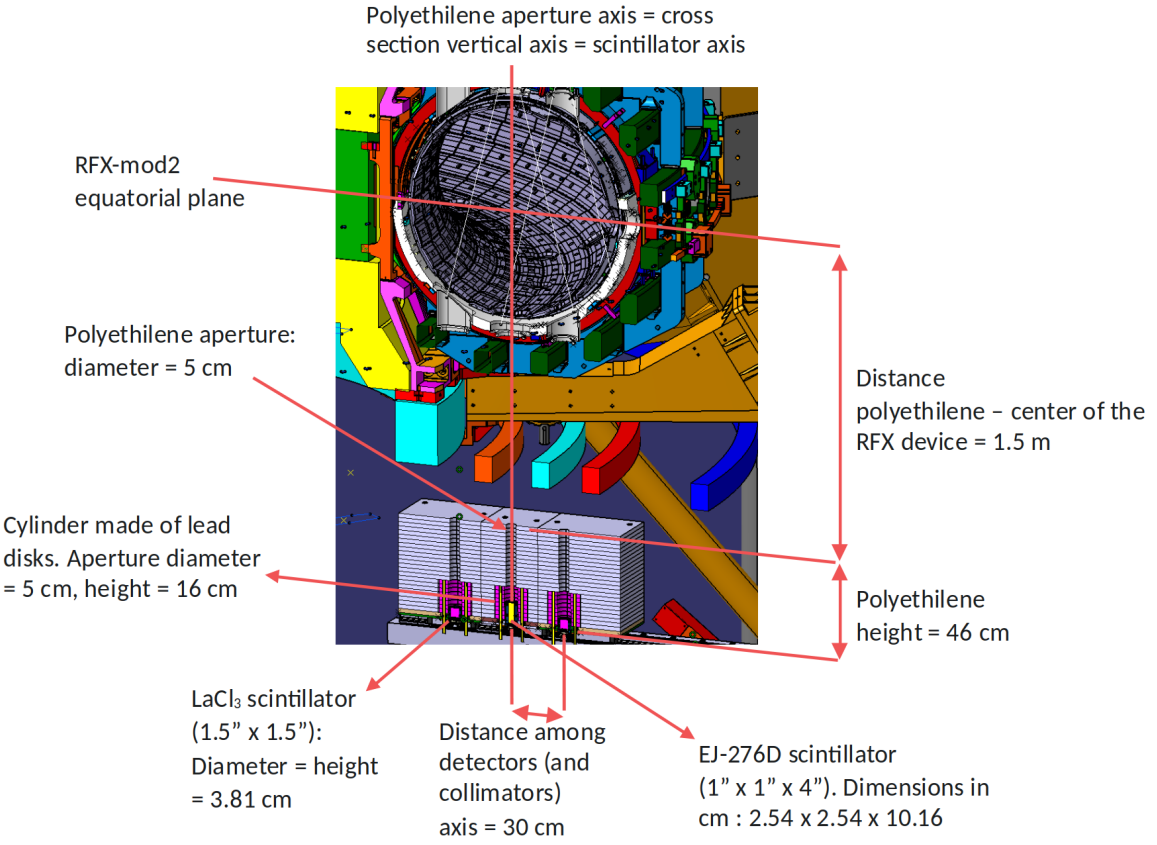

Figure 2. Main geometrical parameters and CAD representation of the neutron/gamma diagnostic. The shielding aperture coincides with the vertical axis of the RFX-mod2 poloidal section and with the axis of the central scintillator.

the shielding and the detectors with the view ports while avoiding the high weight of the entire shielding structure.[5] For the alignment during installation, the shielding placeholders will be placed on a movable tray on rails. Then, the full shielding structure will be assembled and the detectors will be inserted from the bottom accesses shown in figure 3. These bottom accesses will also allow for detector replacement after installation without the need of removing the shielding structure. This should be particularly advantageous in case of fault and to change detector type between EJ-276D and $LaCl_3$:Ce (e.g., during the shutdown phases of RFX-mod2).

3.4 High magnetic field at the detectors location

At the detector locations, it is expected that the magnetic field could reach ~hundreds of mT. Conventional photomultiplier tubes (PMTs) are highly sensitive to magnetic fields, with performance degradation observed even at the level of the Earth's magnetic field (~ 0.05 mT) [27, 37]. Therefore, the magnetic shielding required for a PMT would require a bulky and complex assembly. For reference, the shielding foreseen for the ITER Radial Gamma Ray Spectrometer [38] (which will operate under a comparable magnetic field intensity) has a total mass of ~ 100 kg, with a total thickness of ~5 cm and a length of ~ 50 cm. Implementing comparable shielding at RFX-mod2 would

[5]The total mass of the full structure is expected to be on the order of 100 kg.

2026 JINST 21 C05003

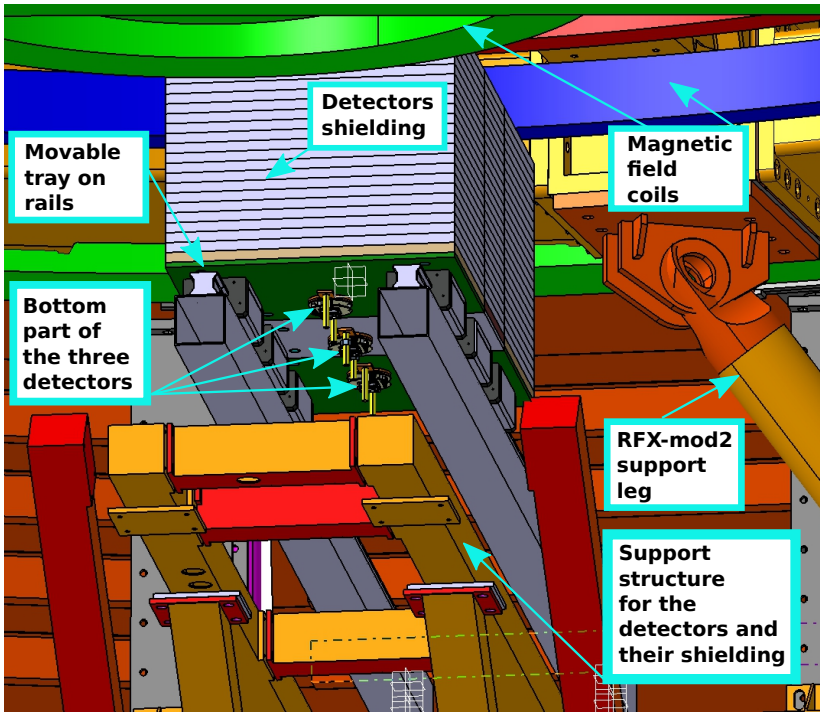

Figure 3. Bottom view of the CAD model assembly, showing the support structure for the neutron/gamma detectors, their shielding, and the accessible region for the detectors. The support structure will be used to hold the detectors and their shielding, so that they are placed as close as possible (within the engineering constraints) to the RFX-mod2 device.

substantially increase mechanical complexity, cost, and occupied volume, potentially compromising the availability of three LOSs.

An alternative could be represented by the use of flat-panel photomultiplier tubes with minimal magnetic shielding, as previously done at RFX-mod and MST (sections 2.1 and 2.2). However, the occurrence of silent phases in past RFX-mod measurements (section 2.3), along with the absence of a definitive explanation for their origin, suggested the adoption of a cautious approach. The latter is represented by the use of Silicon Photomultipliers (SiPMs) as photodetectors for the RFX-mod2 scintillators. Indeed, SiPMs are recognized for their inherent insensitivity to magnetic fields, eliminating the need of bulky shielding structures. In addition, SiPMs are smaller than PMTs, leading to more compact detectors [27].

3.5 Photodetectors

The SiPMs foreseen for RFX-mod2 are matrices of multiple Hamamatsu S13361-3050NE-04 [39].

Even though SiPMs are advantageous for high magnetic field environments, they introduce specific challenges: their gain is highly sensible to temperature variations, their response exhibit non-linearities at excessive signal amplitudes or excessive rates, and their intrinsic slower timing characteristics can increase the pile-up probability and may affect pulse-shape discrimination [27]. Nevertheless, these aspects were examined in prior studies and dedicated solutions were implemented [40, 41].

2026 JINST 21 C05003

A dedicated electronic readout circuit was developed and was already tested in several experiments [42–45]. It used a pole-zero cancellation circuit[6] to obtain faster signal pulses, resulting in a reduced pile-up probability [27, 45].

In ref. [45], a temperature sensor was placed on the back of the SiPM to track its temperature variation over extended periods of time. During the detector characterization phase, the dependence of the SiPM breakdown voltage on temperature can be experimentally determined to obtain a calibration function. Once the operating temperature is known, this calibration function can be used to apply an online correction of the detector gain (e.g., during inter-shot intervals of RFX-mod2).

For RFX-mod2, the planned strategy is to apply this method to compensate for temperature-induced gain shifts. In addition, a Light Emitting Diode (LED) will be used to generate a stable reference peak in the energy spectrum measured with the detector. This should provide validation and monitoring of the temperature correction over an extended period of time.

If significant variations in the LED peak position were to be observed, then, a feedback control loop could be used to maintain the peak position fixed through adjustments of the SiPM bias voltage. In this way, it should be possible to compensate for gain variations arising from effects not necessarily related to the temperature dependence of the SiPM breakdown voltage. This procedure can be performed, for instance, during the inter-shot interval preceding each plasma discharge.

Both compensation methods assume that the gain remains sufficiently stable during a plasma discharge (since the latter is expected to have a maximum duration of less than 500 ms). Nevertheless, to test this assumption, the LED will be switched-on during representative plasma discharges of RFX-mod2 to track its corresponding peak position in the energy spectrum.

Finally, the non-linear response of the photodetector (SiPM) at high energies could be characterized as a function of count rate using the methodology presented in [45], leading to the derivation of an appropriate calibration curve. This calibration can be applied offline to correct the measured energy spectrum. Nevertheless, in [45], the detector response was found to be effectively linear below 3 MeV. Therefore, for RFX-mod2, preliminary measurements may reveal that this correction is not strictly necessary.

3.6 Prototype detector

The implementation of the pole-zero cancellation in the SiPM readout circuit comes with a modification of the signals shape, which can potentially have a negative impact on the PSD performance of the system [46]. To address this concern, the PSD performance of a prototype detector, consisting of an EJ-276D scintillator coupled to a Hamamatsu S13361-3050NE-04 [39] SiPM,[7] were experimentally assessed in ref. [27]. In that work, neutron data were not yet available. Therefore, only results for alpha/gamma discrimination were presented, along with the use of gamma-ray laboratory sources to calibrate the detector in MeV-electron-equivalent (MeVee) energy units. In the work presented in section 4 of this paper, the same detector and calibration function were used to experimentally assess its neutron/gamma discrimination capabilities.

The prototype detector is not only useful to test the PSD performance with the foreseen setup, but also to obtain preliminary experimental information at RFX-mod2 prior to finalizing the diagnostic

[6] Its original design and working principle can be found in [46]. For the detectors described in refs. [41, 45], and for the EJ-276D detector prototype discussed in sections 3.6 and 4, an improved version of the readout circuit was used.

[7] I.e., the same SiPM model that will be used for the detectors of the RFX-mod2 neutron/gamma diagnostic.

2026 JINST 21 C05003

design. At present, estimates of the expected particle rate at the detectors are affected by large uncertainty, primarily due to the lack of reliable neutron/gamma measurements for RFX-mod and the strong and non-linear energy dependence of the d(d,n)^{3}He reaction cross-section. As a result, existing predictions have limited quantitative reliability. For this reason, estimates of the neutron/gamma fluxes (and possibly the gamma-ray energy spectrum) during the first deuterium plasma campaing at RFX-mod2 are considered necessary before the installation of the final diagnostic system.

4 Characterization of the prototype detector for neutron measurements

4.1 Neutron dataset and energy spectrum

Data were acquired at the Frascati Neutron Generator (FNG) [47, 48] with the EJ-276D-based prototype detector. At FNG, deuterons were accelerated up to 300 keV in a linear electrostatic accelerator and directed onto a tritiated titanium target, producing a high neutron yield ($\sim 10^{11}$ n/s) of ~14 MeV neutrons via the d(t,n)α fusion reaction [48]. Full waveforms were collected with the prototype detector for each trigger-event, constituting the "*Neutron Dataset*". The energy spectrum of the *Neutron Dataset* is shown in figure 4 and exhibits a broad continuum extending up to the kinematic endpoint. This behavior was expected even though incident neutrons could be approximated as mono-energetic ($\sim$ 14 MeV). Such a shape is consistent with neutron interactions dominated by elastic scattering on Hydrogen and Carbon, which produce recoil nuclei that release energy in the scintillator volume [30, 32].

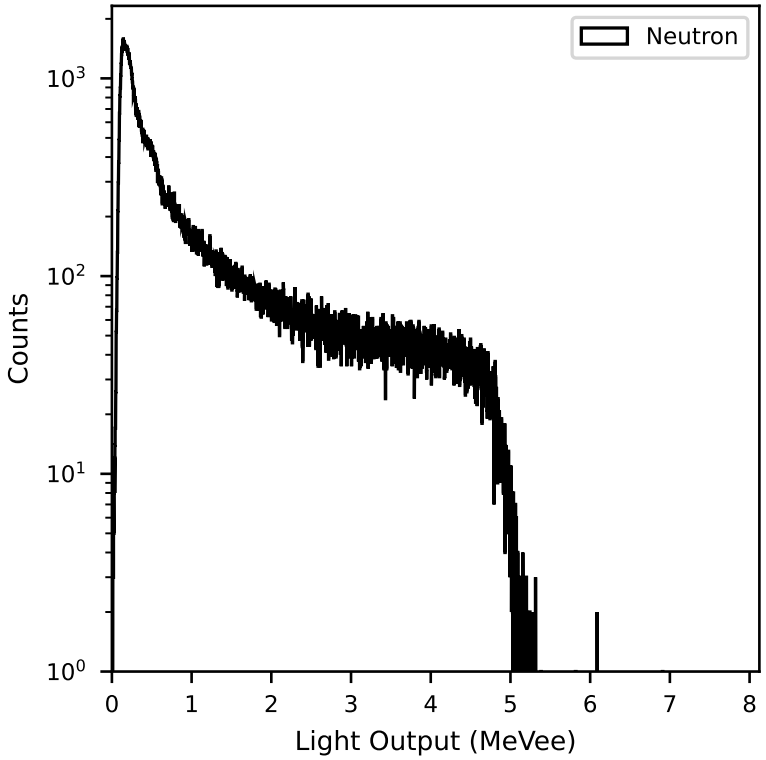

Figure 4. Energy spectrum of the *Neutron Dataset*, measured at FNG with the EJ-276D-based prototype detector.

2026 JINST 21 C05003

4.2 Neutron/gamma discrimination performance

In ref. [27], a dataset collected through measurements with gamma-ray laboratory sources was used to calibrate the prototype detector in Mega-electron-Volt-electron-equivalent units (MeVee). This dataset will hereafter referred to as the "*Gamma Dataset*". In ref. [27] an alpha/gamma discrimination test was also performed, combining the *Gamma Dataset* with another dataset that will hereafter referred to as the "*Alpha Dataset*". The latter was collected through the use of a ^{241}Am laboratory source.

To perform the alpha/gamma discrimination test, for each event that triggered the digitizer acquisition, the full waveform $V(t)$ was recorded, together with the trigger time t_{tr} and the Q_{long}, Q_{short} parameters. These quantities were computed by numerical integration of the waveform over two different time windows:

$$\begin{aligned} Q_{\mathrm{long}} &= \int_{t_0}^{t_0+T_l} V_b(t)\,\mathrm{d}t, \\ Q_{\mathrm{short}} &= \int_{t_0}^{t_0+T_s} V_b(t)\,\mathrm{d}t, \end{aligned} \tag{4.1}$$

where:

- $V_b(t)$ is the waveform after the application of a baseline removal procedure.
- $t_0 = t_{\mathrm{tr}} - T_{\mathrm{pre}}$,
- $T_{\mathrm{pre}} = 50\,\mathrm{ns}$ is the pre-gate temporal window,
- $T_l = 300\,\mathrm{ns}$ is the long-gate temporal window,
- $T_s = 70\,\mathrm{ns}$ is the short-gate temporal window.

Particle identification relied on the PSD parameter, defined as:

$$\mathrm{PSD} = \frac{Q_{\mathrm{long}} - Q_{\mathrm{short}}}{Q_{\mathrm{long}}}\,. \tag{4.2}$$

On the other hand, in the work presented in this paper, the *Gamma Dataset* was used in combination with the *Neutron Dataset* to test the neutron/gamma discrimination capability of the detector, using a procedure analogous to that described above.

Pile-up affected waveforms can mimic the PSD values associated to single event pulses, leading to a degradation of PSD performance. Therefore, before performing the test, pile-up was mitigated using the *find_peaks* Python function [49, 50] applied in post-processing to the each collected waveform: every time two or more event-peaks were found in a waveform, the latter was rejected.

The PSD-energy matrix (reporting the number of waveforms in a given two-dimensional bin determined by the PSD and the energy-electron-equivalent values) is shown in figure 5. PSD performance was evaluated as follows: the PSD-energy matrix was integrated over energy from 0.2 MeVee upward, yielding a 1D histogram (figure 6). The latter was fitted with a Gaussian function to determine the centroid and FWHM of the distribution. These parameters, along with those calculated for the *Gamma Dataset*, were used to compute the following figure of merit:

$$\mathrm{FoM}_{n/g} = \frac{d_{n/g}}{\mathrm{FWHM_n} + \mathrm{FWHM_g}}\,, \tag{4.3}$$

2026 JINST 21 C05003

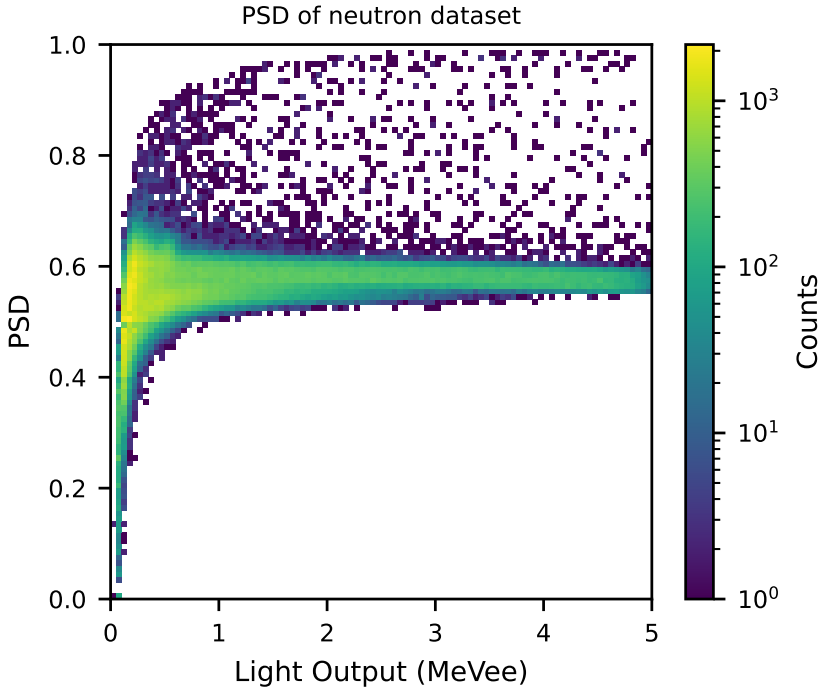

Figure 5. PSD vs. energy (in MeVee units) for the *Neutron Dataset*.

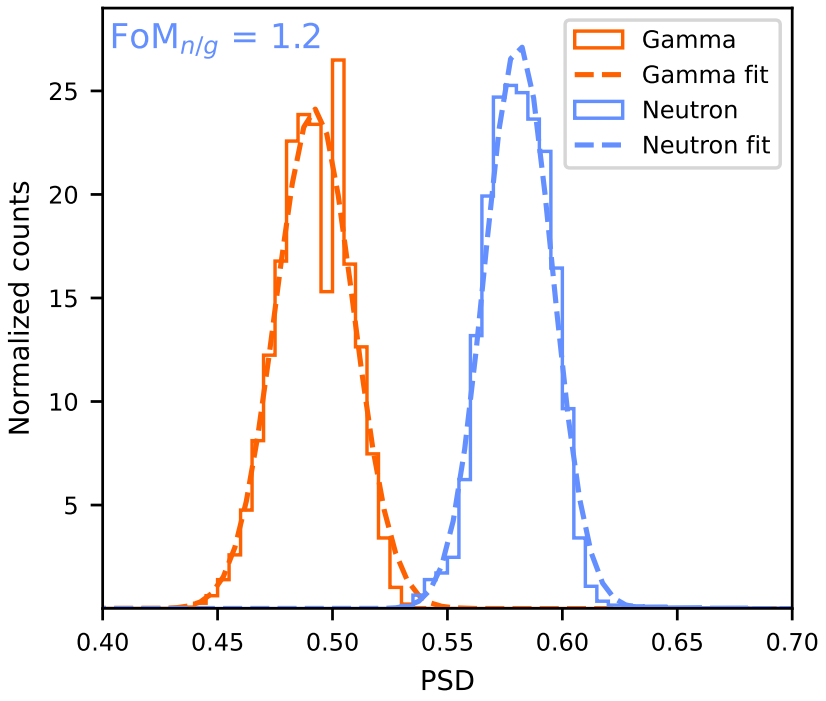

Figure 6. Histograms of PSD values for energies above 0.2 MeVee for the *Gamma Dataset* (orange) and the *Neutron Dataset* (light-blue). The left tail of the light-blue histogram indicates a small contribution of gamma-rays in the *Neutron Dataset*, which can slightly increase the FWHM and result in a slightly lower value of the computed FoM$_{n/g}$ (shown in the upper left corner).

2026 JINST 21 C05003

where $d_{n/g}$ is the separation between the two centroids of the *Neutron* and *Gamma* distributions. $\mathrm{FWHM_n}$ and $\mathrm{FWHM_g}$ are the full widths at half maximum of the *Neutron* and *Gamma* distributions, respectively. The resulting value was

$$\mathrm{FoM}_{n/g} = 1.2\,,$$

indicating good PSD performance despite the presence of residual pile-up and gamma waveforms in the *Neutron Dataset*, both expected to reduce the $\mathrm{FoM}_{n/g}$ value with respect to the ideal case. Therefore, the satisfactory result obtained suggests that the PSD method remains effective even under these adverse testing conditions.

For comparison, the FoM obtained for the *Gamma* and *Alpha* datasets and reported in ref. [27] was

$$\mathrm{FoM}_{a/g} = 1.0\,.$$

4.3 Characterization of the fast and slow components of the signal for each particle type

To gain additional insights into the PSD capabilities of the system, the fast (τ_f) and slow (τ_s) components of the signals coming from the *Neutron, Gamma* and *Alpha* datasets were analyzed by fitting a double-exponential decay to an average of 100 energy-equivalent pulses (for each dataset). The results are shown in figure 7.

The key result is that gamma-induced signals exhibit statistically different fast and slow components compared to those induced by neutrons or alpha particles, providing additional evidence suggesting good PSD capabilities.

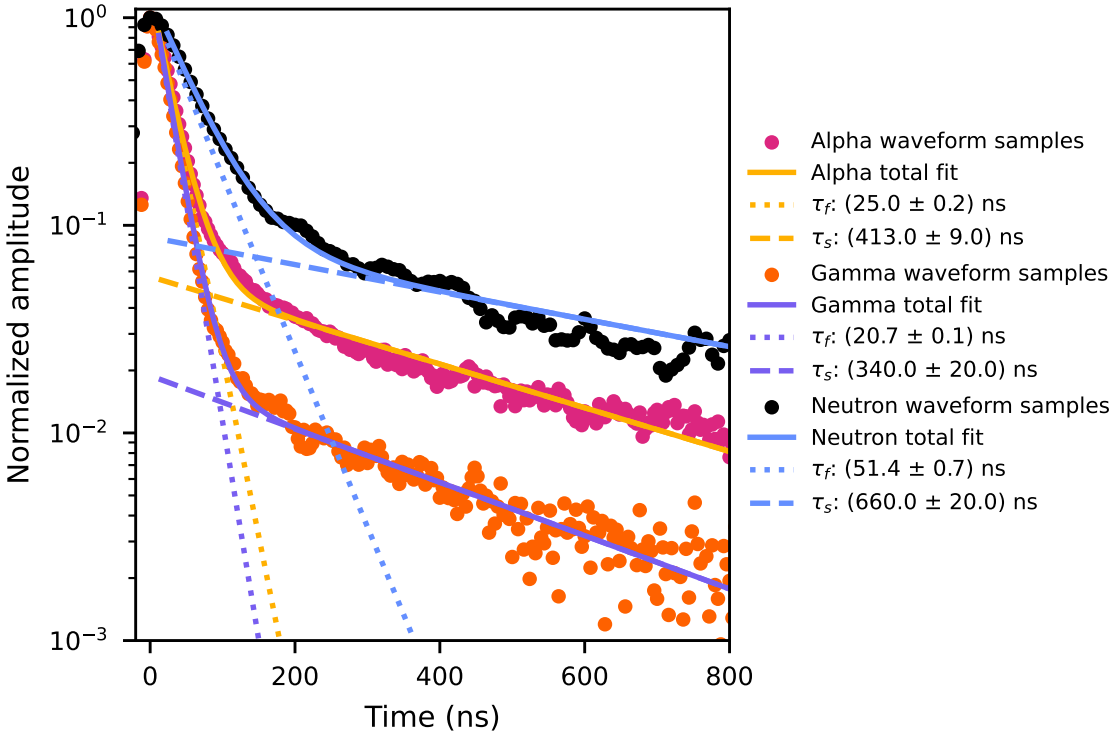

Figure 7. Average voltage pulses for gamma, alpha, and neutron events recorded with the EJ-276D-based prototype detector. The exponential decay fits, as well as the fast (τ_f) and slow (τ_s) signal components resulting from the fit, are shown.

2026 JINST 21 C05003

5 Conclusions

The proposed neutron/gamma diagnostic is expected to be installed in the same poloidal sector of the SXR-GEM at RFX-mod2. A basic level of spatial resolution will be obtained through the use of three lines of sight. This setup should allow simultaneous measurements of SXR, neutrons, and gamma rates on a common spatial and temporal basis, providing simultaneous information on ion and electron acceleration during magnetic reconnection (MR) events to investigate possible correlations.

Measurements will be resolved in energy and time, thanks to the use of two interchangeable types of scintillators: EJ-276D, used specifically for counting, and $LaCl_3$:Ce, used specifically for spectroscopy. The neutron/gamma diagnostic could in principle provide sub-ms temporal resolution. However, in practice, the achievable temporal resolution may be limited by the RFX-mod2 emissivity and the resulting radiation fluxes at the detector positions, which may be insufficient to achieve adequate counting statistics on millisecond or sub-millisecond time scales. To obtain experimental estimates of the radiation fluxes at the detector positions, a prototype detector will be installed during the first deuterium plasma campaign at RFX-mod2. These measurements could enable more reliable, experimentally informed estimates of the achievable temporal resolution of the proposed neutron/gamma diagnostic system and support a subsequent evaluation of its design, which could indicate the need for refinement or confirm its adequacy.

The prototype detector was experimentally characterized in this paper. A figure of merit of 1.2 was obtained for neutron/gamma discrimination. Moreover, gamma-induced signals exhibited statistically different fast and slow components compared to those induced by neutrons or alpha particles. These results suggest that the system is able to discriminate neutron-induced signals form gamma-induced signals in a satisfactory way. Therefore, the prototype detector is considered ready to deployment at RFX-mod2.

While the main experimental target of the neutron/gamma diagnostic is the study of MR events, gamma-ray spectroscopy with spatial information could also be useful to study runaway electrons in future RFX-mod2 tokamak discharges. Moreover, neutron rate measurements could be used to estimate the neutron yield and possibly relate it to fusion power or safety-related aspects.

Acknowledgments

This work is based on Federico Guiotto's PhD thesis in "Fusion Science and Engineering", submitted to the University of Padova on February 2, 2026. At the time of writing, the thesis is under review and is not publicly available.

This work has been carried out within the framework of Italian National Recovery and Resilience Plan (NRRP), funded by the European Union - NextGenerationEU (Mission 4, Component 2, Investment 3.1 - Area ESFRI Energy - Call for tender No. 3264 of 28-12-2021 of Italian University and Research Ministry (MUR), Project ID IR0000007, MUR Concession Decree No. 243 del 04/08/2022, CUP B53C22003070006, "NEFERTARI — New Equipment for Fusion Experimental Research and Technological Advancements with Rfx Infrastructure"). Views and opinions expressed are however those of the author(s) only and do not necessarily reflect those of the European Union or the European Commission. Neither the European Union nor the European Commission can be held responsible for them.

2026 JINST 21 C05003

References

[1] M. Yamada, R. Kulsrud and H. Ji, *Magnetic reconnection*, *Rev. Mod. Phys.* **82** (2010) 603.

[2] F.F. Chen, *Introduction to Plasma Physics and Controlled Fusion*, Springer (1984) [DOI:10.1007/978-1-4757-5595-4].

[3] A. Lazarian, G.L. Eyink, E.T. Vishniac and G. Kowal, *Turbulent Reconnection and Its Implications*, *Phil. Trans. Roy. Soc. Lond. A* **373** (2015) 20140144 [arXiv:1502.01396].

[4] M. Veranda et al., *Magnetic reconnection in three-dimensional quasi-helical pinches*, *Rend. Lincei Sci. Fis. Nat.* **31** (2020) 963.

[5] P.V. Savrukhin, *Generation of Suprathermal Electrons during Magnetic Reconnection at the Sawtooth Crash and Disruption Instability in the T-10 Tokamak*, *Phys. Rev. Lett.* **86** (2001) 3036.

[6] A. Zocco et al., *W7-X and the sawtooth instability: towards realistic simulations of current-driven magnetic reconnection*, *Nucl. Fusion* **61** (2021) 086001.

[7] L. Marrelli et al., *The reversed field pinch*, *Nucl. Fusion* **61** (2021) 023001.

[8] P. Piovesan et al., *RFX-mod: A multi-configuration fusion facility for three-dimensional physics studies*, *Phys. Plasmas* **20** (2013) 056112.

[9] R.N. Dexter et al., *The Madison Symmetric Torus*, *Fusion Technol.* **19** (1991) 131.

[10] B. Momo et al., *The phenomenology of reconnection events in the reversed field pinch*, *Nucl. Fusion* **60** (2020) 056023.

[11] R.M. Magee et al., *Anisotropic Ion Heating and Tail Generation during Tearing Mode Magnetic Reconnection in a High-Temperature Plasma*, *Phys. Rev. Lett.* **107** (2011) 065005.

[12] L. Cordaro et al., *Neutron-gamma measurements at the madison symmetric torus*, in the proceedings of the *2nd Asia-Pacific Conference on Plasma Physics (AAPPS-DPP2018)*, Kanazawa, Japan (2018), p. MFP-24 [https://www.aappsdpp.org/DPP2018Program/pdf/MFP-24.pdf].

[13] A.M. DuBois, J.D. Lee and A.F. Almagri, *A high time resolution x-ray diagnostic on the madison symmetric torus*, *Rev. Sci. Instrum.* **86** (2015) 073512.

[14] A.M. DuBois et al., *Anisotropic Electron Tail Generation during Tearing Mode Magnetic Reconnection*, *Phys. Rev. Lett.* **118** (2017) 075001.

[15] M. Gobbin et al., *Ion heating and energy balance during magnetic reconnection events in the RFX-mod experiment*, *Nucl. Fusion* **62** (2022) 026030.

[16] M. Zuin et al., *Characterization of particle dynamics and magnetic reconnection in the RFX-mod plasmas*, in the proceedings of the *42nd EPS Conference on Plasma Physics*, Lisbon, Portugal, European Physical Society (2015).

[17] W.A. Gonzalez, *Study, development and analysis of In-vessel pick-up coil sensors for ITER magnetic diagnostic and n & gamma detection in fusion plasmas*, Ph.D. Thesis, Università degli Studi di Padova, Padova, Italy (2014) [https://www.research.unipd.it/handle/11577/3424759].

[18] S. Peruzzo et al., *The new vessel complex for the RFX-mod2 experiment: An effective synergy between fusion research and technological development*, *Fusion Eng. Des.* **194** (2023) 113890.

[19] D. Terranova et al., *RFX-mod2 as a flexible device for reversed-field-pinch and low-field tokamak research*, *Nucl. Fusion* **64** (2024) 076003.

[20] M. Zuin et al., *Dynamics of ultralow-q plasmas in the RFX-mod device*, *Nucl. Fusion* **62** (2022) 066029.

2026 JINST 21 C05003

[21] D. Bonfiglio et al., *3D nonlinear MHD simulations of ultra-low q plasmas*, *Nucl. Fusion* **48** (2008) 115010.

[22] M. Puiatti et al., *Extended scenarios opened by the upgrades of the RFX-mod experiment*, in the proceedings of the *26th IAEA Fusion Energy Conference. Programme, Abstracts and Conference Material (IAEA-CN–234)*, Kyoto, Japan (2018), p. 319–319 [https://conferences.iaea.org/event/98/contributions/12310/].

[23] L. Carraro et al., *RFX-mod2 diagnostic capability enhancements for the exploration of multi-magnetic-configurations*, *Nucl. Fusion* **64** (2024) 076032.

[24] F. Guiotto et al., *Development of a GEM based diagnostic for soft x-ray measurements resolved in space, time, and energy at RFX-mod2*, *Plasma Phys. Control. Fusion* **67** (2025) 125013.

[25] Eljen Technology, *EJ-301, EJ-309: Neutron/Gamma PSD Liquid Scintillators*, https://eljentechnology.com/products/liquid-scintillators/ej-301-ej-309 (2021).

[26] G.F. Knoll, *Radiation detection and measurement*, John Wiley & Sons (2010).

[27] A.D. Molin et al., *Development of fast 2.5 MeV neutron detectors for high-intensity stray magnetic field environments*, *Rev. Sci. Instrum.* **95** (2024) 083544.

[28] M. Grodzicka-Kobylka et al., *Fast neutron and gamma ray pulse shape discrimination in EJ-276 and EJ-276G plastic scintillators*, 2020 *JINST* **15** P03030.

[29] M. Grodzicka-Kobylka et al., *Comparison of detectors with pulse shape discrimination capability for simultaneous detection of gamma-rays, slow and fast neutrons*, *Nucl. Instrum. Meth. A* **1019** (2021) 165858.

[30] K.D. Ngo et al., *Fast neutron response characterization of an EJ-276 plastic scintillator for use as a neutron monitor*, *Nucl. Instrum. Meth. A* **1051** (2023) 168216.

[31] E.V. Pagano et al., *Experimental characterization of discrimination capabilities of EJ-276 and EJ-276G read by SiPM by pulse-shape analysis techniques*, *Nucl. Instrum. Meth. A* **1064** (2024) 169425.

[32] D. Rigamonti et al., *A chlorine based detector ($LaCl_3(Ce)$) for 2.5 MeV neutron spectroscopy in deuterium nuclear fusion plasmas with enhanced particle discrimination algorithm*, *Meas. Sci. Technol.* **36** (2024) 015907.

[33] A. Pankratenko et al., *Neutron spectroscopy with $LaCl_3(Ce)$-based detector on EAST tokamak*, *Fusion Eng. Des.* **218** (2025) 115236.

[34] T.M. Kormilitsyn et al., *Novel $LaCl_3(Ce)$-based spectrometer for deuterium plasma neutron diagnostics*, *Rev. Sci. Instrum.* **92** (2021) 043528.

[35] R. Bernabei et al., *Performances and potentialities of a $LaCl_3$:Ce scintillator*, *Nucl. Instrum. Meth. A* **555** (2005) 270.

[36] Dassault Systèmes, *CATIA*, https://www.3ds.com/products/catia (2025).

[37] Hamamatsu Photonics K.K., *Photomultiplier Tubes: Basics and Applications*, Hamamatsu Photonics K.K., Electron Tube Division, Hamamatsu, Japan, fourth ed. (2017).

[38] F. Scioscioli et al., *Design and development status of the ITER Radial Gamma Ray Spectrometer*, *Fusion Eng. Des.* **221** (2025) 115376.

[39] Hamamatsu Photonics K.K., *MPPC Array S13361-3050NE-04 Data Sheet*, Product Specification Sheet, https://www.hamamatsu.com/jp/en/product/optical-sensors/mppc/mppc_mppc-array/S13361-3050NE-04.html (2025).

2026 JINST 21 C05003

[40] A. Dal Molin et al., *Development of a new compact gamma-ray spectrometer optimised for runaway electron measurements*, *Rev. Sci. Instrum.* **89** (2018) 10I134.

[41] A. Lvovskiy et al., *Upgrades to the gamma ray imager on DIII-D enabling access to high flux hard x-ray measurements during the runaway electron plateau phase (invited)*, *Rev. Sci. Instrum.* **93** (2022) 113524.

[42] M. Nocente et al., *Gamma-ray spectroscopy at mhz counting rates with $LaBr_3$ scintillators for fusion plasma diagnostics*, *Rev. Sci. Instrum.* **87** (2016) 11E714.

[43] D. Rigamonti et al., *Performance of the prototype LaBr3 spectrometer developed for the JET gamma-ray camera upgrade*, *Rev. Sci. Instrum.* **87** (2016) 11E717.

[44] D. Rigamonti et al., *The upgraded JET gamma-ray cameras based on high resolution/high count rate compact spectrometers*, *Rev. Sci. Instrum.* **89** (2018) 10I116.

[45] A. Dal Molin et al., *Novel compact hard x-ray spectrometer with MCps counting rate capabilities for runaway electron measurements on DIII-D*, *Rev. Sci. Instrum.* **92** (2021) 043517.

[46] M. Nocente et al., *Experimental investigation of silicon photomultipliers as compact light readout systems for gamma-ray spectroscopy applications in fusion plasmas*, *Rev. Sci. Instrum.* **85** (2014) 11E108.

[47] M. Martone, M. Angelone and M. Pillon, *The 14 MeV Frascati neutron generator*, *J. Nucl. Mater.* **212-215** (1994) 1661.

[48] A. Pietropaolo et al., *The Frascati Neutron Generator: A multipurpose facility for physics and engineering*, *J. Phys. Conf. Ser.* **1021** (2018) 012004.

[49] SciPy Community, *scipy.signal.find_peaks: SciPy v1.14.1 Documentation*, `https://docs.scipy.org/doc/scipy/reference/generated/scipy.signal.find_peaks.html` (2024).

[50] Python Software Foundation, *Python Language Reference*, `https://www.python.org` (2025).

2026 JINST 21 C05003